Supplementary Information-Superconductivity in Mo-P Compounds Under Pressure and in Double-Weyl Semimetal Hex-MoP_2

Xin-Hai Tu[abc], Tao Bo[bd], Peng-Fei Liu[ab], Wen Yin[abc], Ning Hao[*e] and Bao-Tian Wang[*abcf]

1 Structural prediction of Mo_xP_y (x=1-3, y=1-4)

The pressure-enthalpy diagram of Mo-P structure is presented in Fig. S1. All these systems are dynamically stable with non-negative phonon modes. Among these structures, we predict five global stable structures and show crystal structures, phonon modes, and band structures of them in Fig. S2. In Table S1, the lattice parameters and the Wyckoff positions of five predicted Mo-P compounds and hex-MoP_2 are sorted out.

2 Superconductivity

From Fig. S3, by and large, the phonon modes of hex-MoP_2 are similar and remain dynamically stable under different concentration of carrier doping except the doping of 0.4 electrons and 0.6 holes. One can see that the electron (hole) doping decreases the phonon soft modes at H (L) point. In Fig. S4, we show superconducting transition temperature of hex-MoP_2 according to concentration of carrier doping. With 0.4 h/cell doping, the temperature is enhanced up to 6.2 K.

The EPC constant $\lambda(\omega)$ is calculated, according to the Migdal-Eliashberg theory[1,2], by the integral of the Eliashberg spectral function $\alpha^2F(\omega)$ or the summation of the EPC $\lambda_{q\nu}$ in the full BZ for all phonon modes as follow,

$$\lambda(\omega) = 2\int_0^{\omega} \frac{\alpha^2F(\omega)}{\omega} \mathrm{d}\omega = \sum_{q\nu} \lambda_{q\nu}, \tag{1}$$

where the Eliashberg spectral function $\alpha^2F(\omega)$ is estimated by

$$\alpha^2F(\omega) = \frac{1}{2\pi N(E_F)} \sum_{q\nu} \frac{\gamma_{q\nu}}{\omega_{q\nu}} \delta(\omega - \omega_{q\nu}), \tag{2}$$

and $\lambda_{q\nu}$ is calculated by

$$\lambda_{q\nu} = \frac{\gamma_{q\nu}}{\pi h N(E_F) \omega_{q\nu}^2}. \tag{3}$$

$\gamma_{q\nu}$ is the phonon linewidth, $\omega_{q\nu}$ is the phonon frequency of the ν^{th} mode at the wave vector q, and $N(E_\mathrm{F})$ is the electronic density of state at the Fermi level E_F. The $\gamma_{q\nu}$ is defined as

$$\gamma_{q\nu} = \frac{2\pi\omega_{q\nu}}{\Omega_{\mathrm{BZ}}} \sum_{\mathbf{k},n,m} |g^{\nu}_{\mathbf{k}n,\mathbf{k}+qm}|^2 \delta(\varepsilon_{\mathbf{k}n} - \varepsilon_\mathrm{F}) \delta(\varepsilon_{\mathbf{k}+qm} - \varepsilon_\mathrm{F}), \tag{4}$$

where Ω_{BZ} is the volume of BZ, $\varepsilon_{\mathbf{k}n}$ and $\varepsilon_{\mathbf{k}+qm}$ denote the Kohn-Sham energy, and $g^{\nu}_{\mathbf{k}n,\mathbf{k}+qm}$ represents the EPC matrix element. The $g^{\nu}_{\mathbf{k}n,\mathbf{k}+qm}$, which can be determined self-consistently by the linear response theory, describes the probability amplitude for the scattering of an electron with a transfer of crystal momentum vector q.

Next, the superconducting transition temperature T_c can be calculated by the McMillan-Allen-Dynes formula

$$T_\mathrm{c} = \frac{\omega_{\log}}{1.2} \exp[-\frac{1.04(1+\lambda)}{\lambda - \mu^*(1+0.62\lambda)}], \tag{5}$$

where $\omega_{\log}$ is the logarithmic average frequency and can be calculated by

$$\omega_{\log} = \exp[\frac{2}{\lambda}\int_0^{\infty} \frac{\mathrm{d}\omega}{\omega} \alpha^2F(\omega)\log\omega]. \tag{6}$$

μ^* is the effective screened Coulomb repulsion constant and can be set to a typical value of 0.1 according to the empirical values of 0.08 to 0.15[3–9].

3 Hybrid functionals

In this section, we discuss the effect of hybrid functional (HF) calculations on WP. From Fig. S5, we can see that the WP is gapped with two different HF HSE06 and PBE0, indicating the WP is non-topologically protected and which results from accidental degeneracy. Under negative pressure, the gap enlarges further, but the WP will appear again under positive pressure up to 10 GPa (Fig. S6). Thus, it is convenient to study topological phase transition in hex-MoP_2. The phonon modes of hex-MoP_2 are similar and remain dynamically stable under different pressure, as shown in Fig. S7.

[0] *The first two authors contributed equally to this work*
[0a] *Institute of High Energy Physics, Chinese Academy of Sciences (CAS), Beijing 100049, China*
[0b] *Spallation Neutron Source Science Center, Institute of High Energy Physics, Chinese Academy of Sciences, Dongguan 523803, China*
[0c] *University of Chinese Academy of Sciences, Beijing 100039, China*
[0d] *Engineering Laboratory of Advanced Energy Materials, Ningbo Institute of Materials Technology & Engineering, Chinese Academy of Sciences (CAS), Ningbo, Zhejiang 315201, China*
[0e] *Anhui Province Key Laboratory of Condensed Matter Physics at Extreme Conditions, High Magnetic Field Laboratory, Chinese Academy of Sciences, Hefei, Anhui 230031, China*
[0f] *Collaborative Innovation Center of Extreme Optics, Shanxi University, Taiyuan, Shanxi 030006, China*

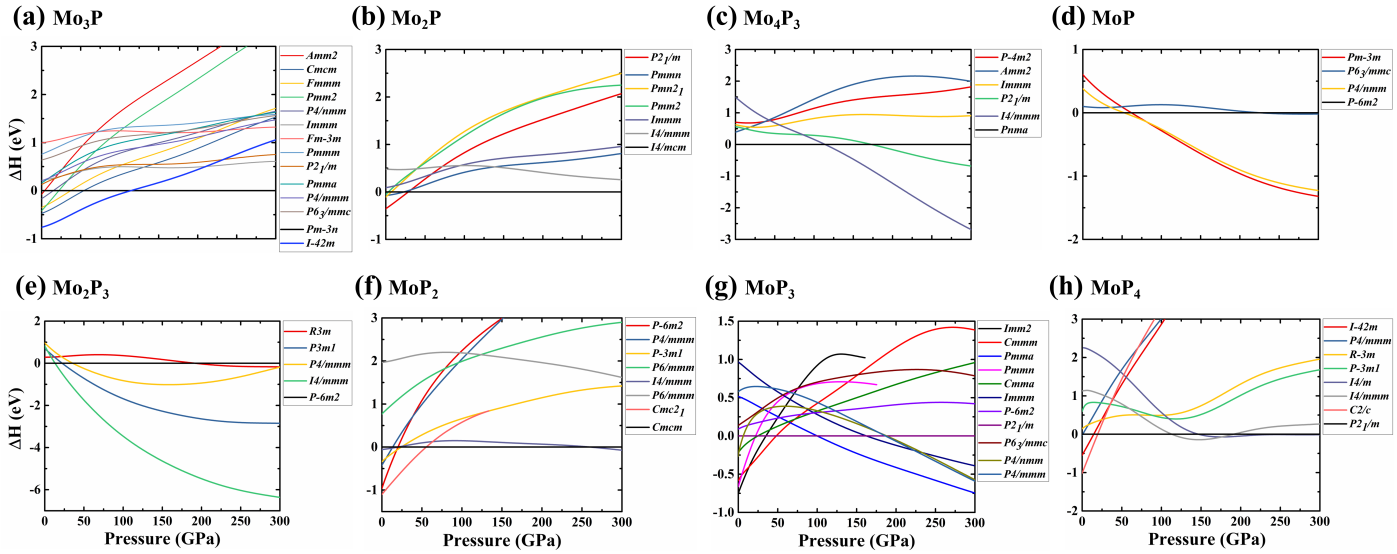

Figure S1 (a)-(h) Calculated enthalpy difference for Mo_3P, Mo_2P, Mo_4P_3, MoP, Mo_2P_3, MoP_2, MoP_3, and MoP_4 at the pressure range of 0-300 GPa. Space groups are shown in different colors.

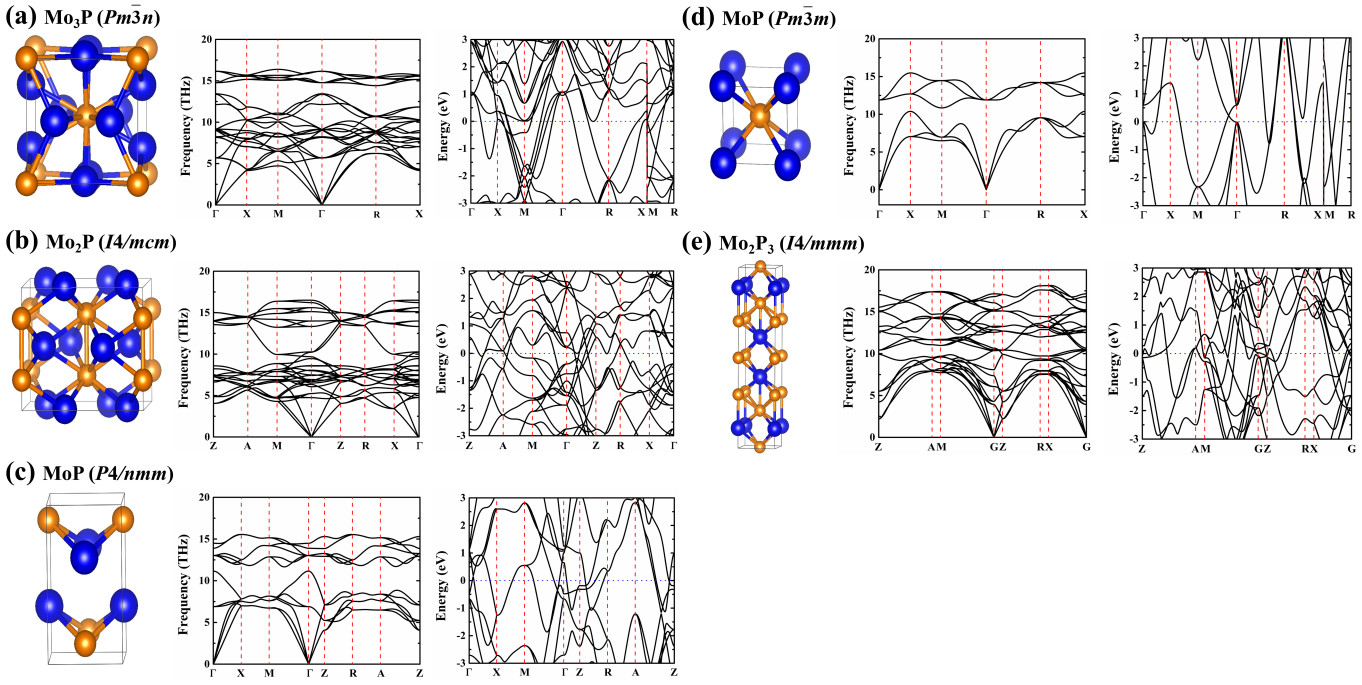

Figure S2 (a)-(e) Crystal structures, phonon modes, and band structures of five global stable Mo_3P ($Pm\bar{3}n$), Mo_2P ($I4/mcm$), MoP ($P4/nmm$ and $Pm\bar{3}m$), and Mo_2P_3 ($I4/mmm$) at 150 GPa, 60 GPa, 60 GPa, 100 GPa, and 100 GPa, respectively. The blue and golden ball are Mo atoms and P atoms, respectively.

Table S1 Pressures, lattice parameters, and Wyckoff positions of five predicted Mo-P compounds and hex-MoP_2.

Compounds	Pressure (GPa)	Lattice parameters (Å)	Wyckoff position
Mo_3P ($Pm\bar{3}n$)	150	$a=b=c=4.393$ $\alpha=\beta=\gamma=90^\circ$	Mo 6*d* 0.000 0.750 0.500 P 2*a* 0.500 0.500 0.500
Mo_2P ($I4/mcm$)	60	$a=b=5.577$ and $c=4.623$ $\alpha=\beta=\gamma=90^\circ$	Mo 8*h* 0.658 0.842 0.500 P 4*a* 0.500 0.500 0.750
MoP ($P4/nmm$)	60	$a=b=2.980$ and $c=5.234$ $\alpha=\beta=\gamma=90^\circ$	Mo 2c 0.5000 0.000 0.330 P 2c 0.000 0.500 0.130
MoP ($Pm\bar{3}m$)	100	$a=b=c=2.773$ $\alpha=\beta=\gamma=90^\circ$	Mo 1a 0.0000 0.000 0.000 P 1b 0.500 0.500 0.500
Mo_2P_3 ($I4/mmm$)	100	$a=b=2.861$ and $c=12.706$ $\alpha=\beta=\gamma=90^\circ$	Mo 4e 0.000 0.000 0.111 P1 4e 0.000 0.000 0.297 P2 2b 0.500 0.500 0.000
hex-MoP_2	0	$a=b=3.345$ and $c=5.106$ $\alpha=90^\circ$, $\beta=90^\circ$, $\gamma=120^\circ$	Mo 1a 0.000 0.000 0.000 P1 1a 0.333 0.667 0.713 P2 1a 0.333 0.667 0.287

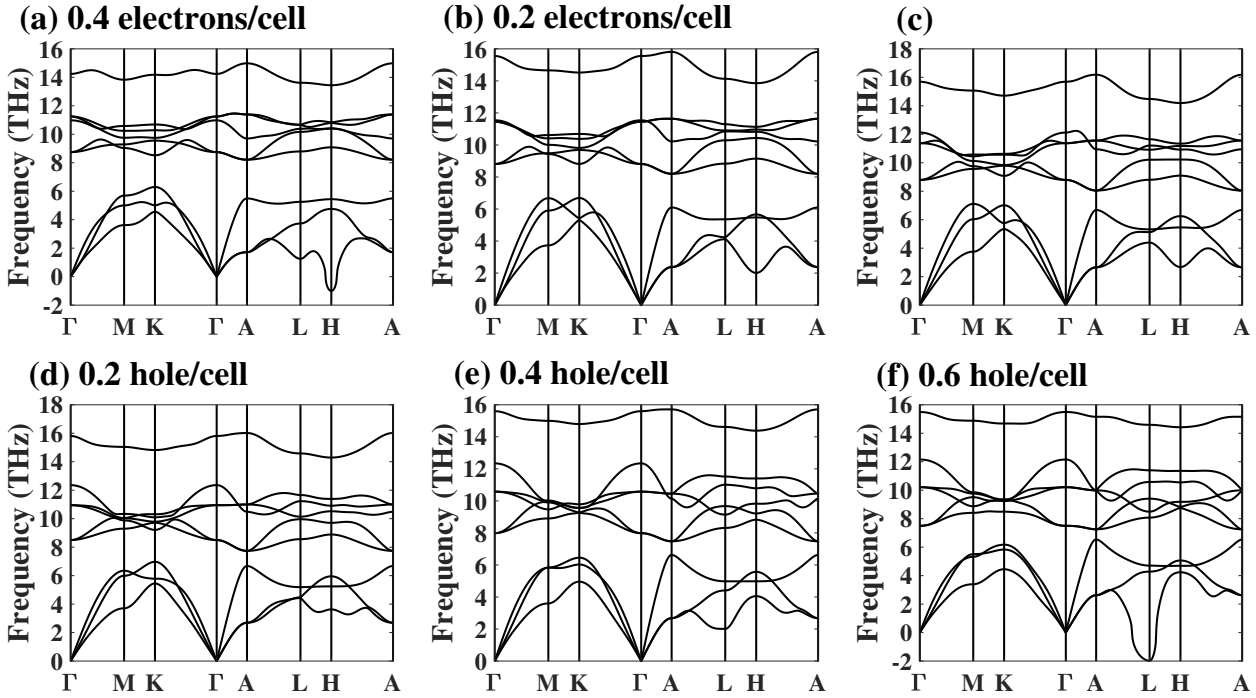

Figure S3 The phonon modes of hex-MoP_2 with regard to concentration of carrier doping.

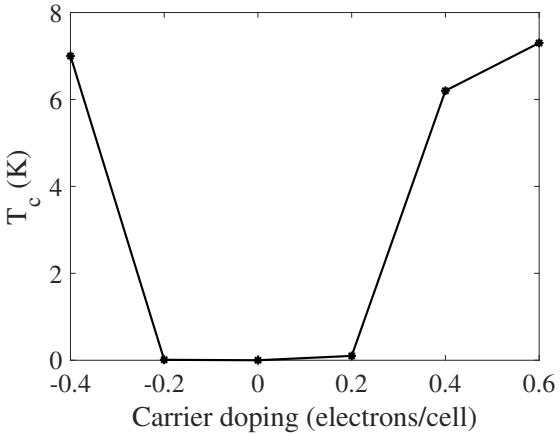

Figure S4 The superconducting transition temperature T_c of hex-MoP_2 according to concentration of carrier doping.

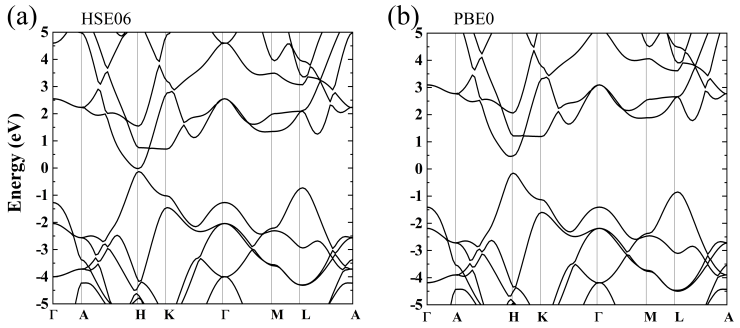

Figure S5 The band structure of hex-MoP_2 with hybrid functionals of HSE06 (a) and PBE0 (b).

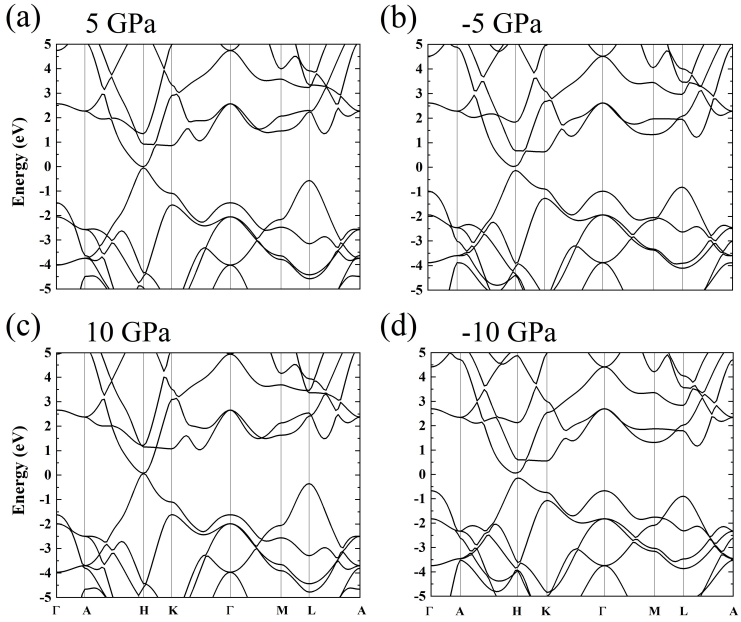

Figure S6 The band structure of hex-MoP_2 with hybrid functionals of HSE06 under different pressure (a) 5 GPa, -5 GPa (b), 10 GPa (c), and -10Gpa (d).

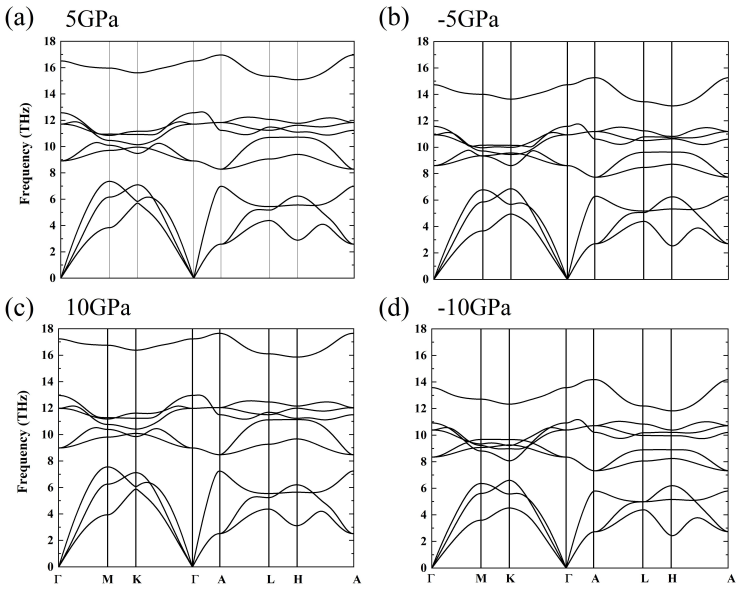

Figure S7 The phonon modes of hex-MoP_2 under different pressure (a) 5 GPa, -5 GPa (b), 10 GPa (c), and -10Gpa (d).

Table S2 Fitting parameters of TBM. εs are the on-site energy and ts are hopping energy. All energy parameters are in units of eV.

Fitting parameters	λ	ε_1	ε_2	t_1	t_2	t_3	t_4	t_5	t_6	
Values	0.05	1.54	-0.19	0.55	0.14	-0.05	-0.16	-0.02	-0.60	
Fitting parameters	t_7	t_8	t_9	t_{10}	t_{11}	t_{12}	t_{13}	t_{14}	t_{15}	t_{16}
Values	-0.31	0.22	0.02	-0.24	-0.09	0.03	-0.06	0.08	0.05	0.00

4 Tight-binding model

We construct a three-band TBM by considering the nearest-neighbor hopping (NNP) in plane and next-NNP out of plane between Mo atoms for hex-MoP_2 under the orbital basis $\{d_{xy},\ d_{x^2-y^2},\ d_{z^2}\}$. The Bloch wave function can be written as follow

$$\left|\tilde{\chi}^{\mathbf{k}}_{\alpha,j}\right\rangle = \frac{1}{\sqrt{N}}\sum_{\mathbf{R}_n} e^{i\mathbf{k}\cdot\mathbf{R}_n}\left|\phi_{\mathbf{R}_n,\alpha,j}\right\rangle, \tag{7}$$

where $\left|\phi_{\mathbf{R}_n,\alpha,j}\right\rangle$ represents the α^{th} atomic orbital of j^{th} atom, $\mathbf{R}_n$ is the lattice vector, and N is the number of primitive cells. The matrix form of Hamiltonian is

$$H^k_{\alpha i,\beta j} \equiv \left\langle \tilde{\chi}^{\mathbf{k}}_{\alpha i}|H|\tilde{\chi}^k_{\beta j}\right\rangle = \sum_{R_n} e^{i\mathbf{k}\cdot R_n} E^{ij}_{\alpha\beta}(R_n), \tag{8}$$

where

$$E^{ij}_{\alpha\beta}(R_n) = \left\langle \phi^i_\alpha(r)|\hat{H}|\phi^j_\beta(r-R_n)\right\rangle \tag{9}$$

is the hopping integral between the atomic orbitals $\left|\phi^i_\alpha\right\rangle$ at $\mathbf{0}$ and $\left|\phi^j_\beta\right\rangle$ at lattice vector R. Given $E^{ij}_{\alpha\beta}(R_n)$, the hopping integrals to all neighboring sites can be generated by

$$E^{ij}_{\alpha\beta}(RR_n) = D^i(R)\,E^{ij}(R_n)\left[D^j(R)\right]^\dagger \tag{10}$$

where $D^i(R)$ is the matrix of the i^{th} irreducible representations and $E^{ij}(R_n)$ is the matrix composed of $E^{ij}_{\alpha\beta}(R_n)$. R is a subset of the symmetry operations of point group. MoP_2 is crystallized in the space group $P\bar{6}M2$ (No. 187) which has the point group D_{3h} symmetry,

$$D_{3h} = \left\{E, 2C_3, 3C_2', \sigma_h, 2S_3, 3\sigma_v\right\}. \tag{11}$$

The final form of Hamiltonian is given by

$$H_0 = \begin{bmatrix} h_{11} & h_{12} & h_{13} \\ & h_{22} & h_{23} \\ h.c. & & h_{33} \end{bmatrix}, \tag{12}$$

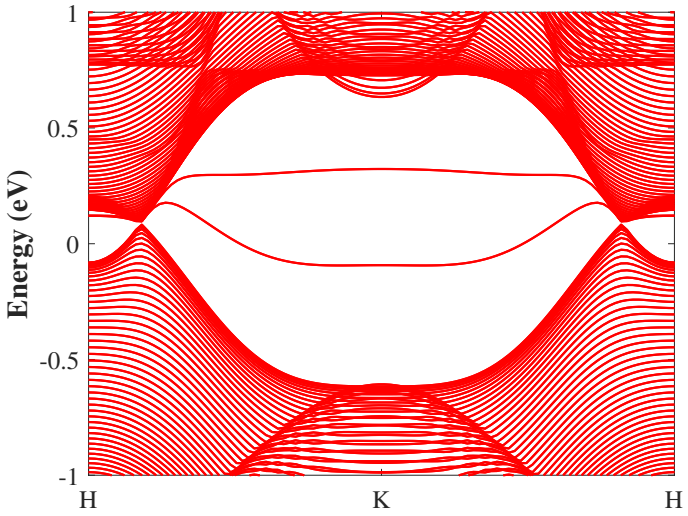

Figure S8 The topological surface states on the (100) surface calculated from TBM.

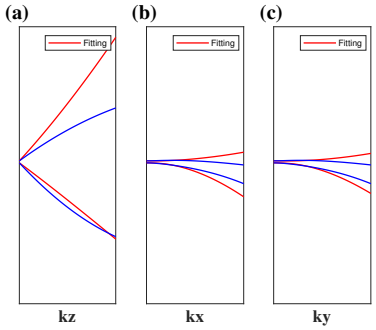

Figure S9 The energy dispersion obtained according to k·p model (red line) is compared with that from first-principles calculations (blue line).

where

$$
\begin{aligned}
h_{11} &= \varepsilon_1 + t_1[2\cos(k_x a) + \cos(\tfrac{1}{2}k_x a)\cos(\tfrac{\sqrt{3}}{2}k_y a)] + 3t_2\cos(\tfrac{1}{2}k_x a)\cos(\tfrac{\sqrt{3}}{2}k_y a) + 2t_3\cos(k_z a) \\
&+2\cos(k_z a)\{t_9[2\cos(k_x a) + \cos(\tfrac{1}{2}k_x a)\cos(\tfrac{\sqrt{3}}{2}k_y a)] + 3t_{10}\cos(\tfrac{1}{2}k_x a)\cos(\tfrac{\sqrt{3}}{2}k_y a)\} + 2t_{15}\cos(2k_z a), \\
h_{12} &= 2it_4[\sin(k_x a) - 2\sin(\tfrac{1}{2}k_x a)\cos(\tfrac{\sqrt{3}}{2}k_y a)] - \sqrt{3}(t_1 - t_2)\sin(\tfrac{1}{2}k_x a)\sin(\tfrac{\sqrt{3}}{2}k_y a) \\
&+2\cos(k_z a)\{2it_{11}[\sin(k_x a) - 2\sin(\tfrac{1}{2}k_x a)\cos(\tfrac{\sqrt{3}}{2}k_y a)] - \sqrt{3}(t_9 - t_{10})\sin(\tfrac{1}{2}k_x a)\sin(\tfrac{\sqrt{3}}{2}k_y a)\}, \\
h_{13} &= 2it_5[\sin(k_x a) + \sin(\tfrac{1}{2}k_x a)\cos(\tfrac{\sqrt{3}}{2}k_y a)] - 2\sqrt{3}t_6\sin(\tfrac{1}{2}k_x a)\sin(\tfrac{\sqrt{3}}{2}k_y a) \\
&+2\cos(k_z a)\{2it_{11}[\sin(k_x a) + \sin(\tfrac{1}{2}k_x a)\cos(\tfrac{\sqrt{3}}{2}k_y a)] - 2\sqrt{3}t_{13}\sin(\tfrac{1}{2}k_x a)\sin(\tfrac{\sqrt{3}}{2}k_y a)\}, \\
h_{22} &= \varepsilon_1 + t_2[2\cos(k_x a) + \cos(\tfrac{1}{2}k_x a)\cos(\tfrac{\sqrt{3}}{2}k_y a)] + 3t_1\cos(\tfrac{1}{2}k_x a)\cos(\tfrac{\sqrt{3}}{2}k_y a) + 2t_3\cos(k_z a) \\
&+2\cos(k_z a)\{t_{10}[2\cos(k_x a) + \cos(\tfrac{1}{2}k_x a)\cos(\tfrac{\sqrt{3}}{2}k_y a)] + 3t_9\cos(\tfrac{1}{2}k_x a)\cos(\tfrac{\sqrt{3}}{2}k_y a)\} + 2t_{15}\cos(2k_z a), \\
h_{23} &= 2t_6[\cos(k_x a) - \cos(\tfrac{1}{2}k_x a)\cos(\tfrac{\sqrt{3}}{2}k_y a)] + 2\sqrt{3}it_5\cos(\tfrac{1}{2}k_x a)\sin(\tfrac{\sqrt{3}}{2}k_y a) \\
&+2\cos(k_z a)\{2t_{13}[\cos(k_x a) - \cos(\tfrac{1}{2}k_x a)\cos(\tfrac{\sqrt{3}}{2}k_y a)] + 2\sqrt{3}it_{12}\cos(\tfrac{1}{2}k_x a)\sin(\tfrac{\sqrt{3}}{2}k_y a)\}, \\
h_{33} &= \varepsilon_2 + t_7[2\cos(k_x a) + 4\cos(\tfrac{1}{2}k_x a)\cos(\tfrac{\sqrt{3}}{2}k_y a)] + 2t_8\cos(k_z a) \\
&+2\cos(k_z a)\{t_{14}[2\cos(k_x a) + 4\cos(\tfrac{1}{2}k_x a)\cos(\tfrac{\sqrt{3}}{2}k_y a)]\} + 2t_{16}\cos(2k_z a),
\end{aligned}
\tag{13}
$$

and εs are on-site energy, ts are hopping energy. The fitting parameters are listed in Table S1.

We show topological surface states on the (100) surface calculated from infinite slabs based on TBM in Fig. S8 which coincides with Fig. 6 (c) and (d).

5 Effective k·p hamiltonian model

Generally, the hamiltonian of a spinless two-band system is in the form of $H(\mathbf{k}) = \sum_{i=0,x,y,z} d_i(\mathbf{k})\sigma_i$ with according eigenvalues $E_\pm = d_0 \pm \sqrt{\mathbf{d}^2}$ and normalized eigen-states,

$$
\psi_\pm = \frac{1}{A_\pm}\begin{pmatrix} \pm\sqrt{\mathbf{d}^2} + d_z \\ d_x + id_y \end{pmatrix}, \tag{14}
$$

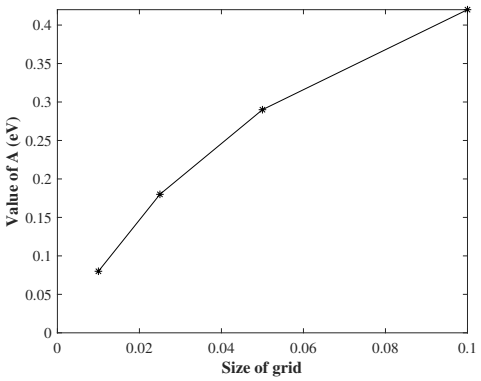

Figure S10 Testing the value of constant A from different size of grids around the DWP.

Table S3 Fitting parameters of k·p model. All energy parameters are in units of eV.

Fitting parameters	m_1	m_2	A	A_1	A_2	B	B_1	B_2	C	C_1	C_2
Values	12.50	0.00	0.00	0.50	-0.33	-0.50	0.32	0.32	-0.10	-0.67	0.15

where σ_0 is the identity matrix, $\sigma_{x,y,z}$ are the three Pauli matrices, and $d_{0,x,y,z}(\mathbf{k})$ are independent real functions of $\mathbf{k}$, $\mathbf{d}^2 = d_x^2 + d_y^2 + d_z^2$, $A_\pm = \sqrt{2(\mathbf{d}^2 \pm d_z\sqrt{\mathbf{d}^2})}$ is normalization constant. Considering d_{xy} and $d_{x^2-y^2}$ as basis, the representations of C_3 and $C_2\mathscr{T}$ operations can be express as

$$\begin{aligned} D(C_3) &= \begin{bmatrix} -\frac{1}{2} & -\frac{\sqrt{3}}{2} \\ \frac{\sqrt{3}}{2} & -\frac{1}{2} \end{bmatrix}, \\ D(C_{2y}\mathscr{T}) &= \begin{bmatrix} -1 & 0 \\ 0 & 1 \end{bmatrix} K, \end{aligned} \tag{15}$$

where K is the complex conjugate operator. Therefore, the 2×2 effective k·p Hamiltonian can be expressed in terms of polynomials of $\mathbf{k}$ through the invariant method as follow:

$$\begin{aligned} H_{eff}(\mathbf{k}) &= [m_1 + Ck_z + C_1(k_x^2 + k_y^2) + C_2 k_z^2]\sigma_0 \\ &+ [Ak_x + A_1 k_x k_z + A_2(k_x^2 - k_y^2)]\sigma_z \\ &- (Ak_y + A_1 k_y k_z - 2A_2 k_x k_y)\sigma_x \\ &+ [m_2 + Bk_z + B_1(k_x^2 + k_y^2) + B_2 k_z^2]\sigma_y, \end{aligned} \tag{16}$$

where σ is Pauli matrix for orbital. The fitting parameters are listed in Table S2 and energy dispersion around the DWP is shown in Fig. S9. To determine whether the value of constant A is zero or not, we test different size of grids around the DWP for fitting. If grid gets smaller, we find the value of A tends to zero. Results are shown in Fig. S10.

6 Monopole charge

The Berry connection and the Berry curvature can be written as,

$$\begin{aligned} \mathbf{A} &= i\langle\psi|\nabla\psi\rangle, \\ \mathbf{F} &= \nabla \times A = i\langle\nabla\psi| \times |\nabla\psi\rangle = i\frac{\langle\psi_+|\nabla H|\psi_-\rangle \times \langle\psi_-|\nabla H|\psi_+\rangle}{(E_+ - E_-)^2}. \end{aligned} \tag{17}$$

For a two-level system, we get general forms of the Berry connection and the Berry curvature as follow,

$$\begin{aligned} A_i &= (2(\mathbf{d}^2 \pm d_z\sqrt{\mathbf{d}^2}))^{-1}(d_y\nabla_i d_x - d_x\nabla_i d_y), \\ F_{ij} &= \frac{1}{2d^3}\varepsilon_{abc} d_a(\nabla_i d_b)(\nabla_j d_c), \end{aligned} \tag{18}$$

where ε_{abc} is 3-dimensional Levi-Civita symbol.

Notes and references

[1] G. Grimvall, *The electron-phonon interaction in metals*, Vol. 8 (North-Holland Amsterdam, 1981).

[2] F. Giustino, Rev. Mod. Phys. **89**, 015003 (2017).

[3] C. F. Richardson and N. W. Ashcroft, Phys. Rev. Lett. **78**, 118 (1997).

[4] K. H. Lee, K. J. Chang, and M. L. Cohen, Phys. Rev. B **52**, 1425 (1995).

[5] J.-J. Zheng and E. R. Margine, Phys. Rev. B **95**, 014512 (2017).

[6] H.-Y. Liu, I. I. Naumov, R. Hoffmann, N. W. Ashcroft, and R. J. Hemley, Proc. Natl. Acad. Sci. USA **114**, 6990 (2017).

[7] B.-T. Wang, P.-F. Liu, J.-J. Zheng, W. Yin, and F.-W. Wang, Phys. Rev. B **98**, 014514 (2018).

[8] P.-F. Liu and B.-T. Wang, J. Mater. Chem. C **6**, 6046 (2018).

[9] L. Yan, P.-F. Liu, H. Li, Y. Tang, J. He, X. Huang, B.-T. Wang, and L. Zhou, **6**, 2057 (2020).